MNRAS **000**, 1–11 (2016) Preprint November 15, 2016 Compiled using MNRAS LATEX style file v3.0

Constraints on shear and rotation with massive galaxy clusters

Ahmad Mehrabi[1] ⋆, Francesco Pace[2], Mohammad Malekjani[1] and Antonino Del Popolo[3,4,5]
[1] *Department of Physics, Bu-Ali Sina University, Hamedan 65178, Iran*
[2] *Jodrell Bank Centre for Astrophysics, School of Physics and Astronomy, The University of Manchester, Manchester, M13 9PL, U.K.*
[3] *Dipartimento di Fisica e Astronomia, Università di Catania, Viale Andrea Doria 6, 95125 Catania, Italy*
[4] *INFN sezione di Catania, Via S. Sofia 64, I-95123 Catania, Italy*
[5] *International Institute of Physics, Universidade Federal do Rio Grande do Norte, Brazil*

arXiv:1608.07961v2 [astro-ph.CO] 14 Nov 2016

Accepted ?, Received ?; in original form November 15, 2016

ABSTRACT

A precise determination of the mass function is an important tool to verify cosmological predictions of the ΛCDM model and to infer more precisely the better model describing the evolution of the Universe. Galaxy clusters have been currently used to infer cosmological parameters, in particular the matter density parameter $\Omega_{\rm m}$, the matter power spectrum normalization σ_8 and the equation of state parameter $w_{\rm de}$ of the dark energy fluid. In this work, using data on massive galaxy clusters ($M > 8 \times 10^{14}\ h^{-1}\ M_{\odot}$) in the redshift range $0.05 \lesssim z \lesssim 0.83$, for the first time we put constraints on the parameter α introduced within the formalism of the extended spherical collapse model to quantify deviations from sphericity due to shear and rotation. Since at the moment there is no physical model describing its functional shape, we assume it to be a logarithmic function of the cluster mass. By holding σ_8 fixed and restricting our analysis to a ΛCDM model, we find, at $1-\sigma$ confidence level, $\Omega_{\rm m} = 0.284 \pm 0.0064$, $h = 0.678 \pm 0.017$ and $\beta = 0.0019^{+0.0008}_{-0.0015}$, where β represents the slope of the parameter α. This results translates into a 9% decrement of the number of massive clusters with respect to a standard ΛCDM mass function, but better data are required to better constrain this quantity, since at the $2-\sigma$ and $3-\sigma$ confidence level we are only able to infer upper limits.

Key words: cosmology: methods: analytical - statistical - cosmology: theory - dark energy

1 INTRODUCTION

It is strongly believed that large scale cosmic structures such as galaxies and clusters of galaxies are originated from small initial fluctuations during the inflationary era (Starobinsky 1980; Guth 1981; Linde 1990). Later, these fluctuations can grow due to gravitational instability (Gunn & Gott 1972; Press & Schechter 1974; White & Rees 1978; Peebles 1993; Del Popolo & Gambera 1998; Peacock 1999; Sheth & Tormen 1999; Barkana & Loeb 2001; Peebles & Ratra 2003; Ciardi & Ferrara 2005; Bromm & Yoshida 2011). Most of the growth of cosmic structures takes place after the decoupling epoch between photons and baryons. At early times, when the amplitude of fluctuations is very small, linear perturbation theory can be safely used to study the evolution of fluctuations. However, at later times, when the amplitude of fluctuations becomes large, linear perturbations theory fails because fluctuations enter in the non-linear regime. Hence, more sophisticated techniques are required. The spherical collapse model (SCM), first introduced by Gunn & Gott (1972), is a simple analytical method to follow the non-linear evolution of the growth of fluctuations on sub-Horizon scales. This model has been widely investigated in literature (Fillmore & Goldreich 1984; Bertschinger 1985; Hoffman & Shaham 1985; Ryden & Gunn 1987; Subramanian et al. 2000; Ascasibar et al. 2004; Williams et al. 2004; Mota & van de Bruck 2004; Maor & Lahav 2005; Basilakos et al. 2009; Del Popolo 2009; Li et al. 2009; Pace et al. 2010; Wintergerst & Pettorino 2010; Pace et al. 2012, 2014a; Naderi et al. 2015; Malekjani et al. 2015). Moreover, in the SCM, the wavelengths of perturbations are much smaller than the Hubble radius and therefore the Pseudo-Newtonian (PN) hydrodynamical equations can be applied in this formalism (Lima et al. 1997). It has been shown that the results of the quoted approach in the linear regime are consistent with general relativity (GR) theory (Abramo et al. 2007, 2009). Recently, the SCM has been extended to more general cases where also the rotation (vorticity) ω, and the shear σ, are taken into account (Del Popolo et al. 2013a,c,b; Pace et al. 2014b). Reischke et al. (2016) instead provided a description of the shear due to tidal shear forces using the Zel'dovich approximation, hence not relying on phenomenological approaches. In particular, Del Popolo et al. (2013c,b) showed that in the presence of shear and rotation, the collapse of structures is slowed down due to the strength of the rotation term, the SCM parameters become mass dependent as in the ellipsoidal collapse (with a stronger dependence on galactic scales).

One of the most important features of the SCM formalism is that it can be used to describe the abundance of col-

⋆ mehrabi@basu.ac.ir

lapsed haloes as a function of mass and redshift (Press & Schechter 1974). Information coming from the abundance of collapsed structures is an important tool to study the distribution of matter in the universe (Evrard et al. 2002). Observationally, the mass function and the number counts of massive galaxy clusters have been inferred through X-ray surveys (Del Popolo & Gambera 1999; Borgani et al. 2001; Reiprich & Boehringer 2002; Vikhlinin et al. 2009a), weak and strong lensing studies (Bartelmann et al. 1998; Dahle 2006; Corless & King 2009; Corless et al. 2009) and optical surveys, like the SDSS (Bahcall et al. 2003a,b,c). It should be noted that the redshift evolution of massive clusters depends strongly on cosmological parameters, especially on the amplitude of mass fluctuations σ_8 and on the non-relativistic matter density parameter Ω_m (Bahcall & Fan 1998; Bahcall & Bode 2003). Higher values of σ_8 favour the formation of haloes at early times, while lower values give rise to fewer massive clusters at high redshifts. In the last two decades, data on the number counts of massive clusters ($M_{\rm cluster} > 8\times10^{14}h^{-1}M_\odot$ in a comoving radius $R_{\rm cluster} = 1.5h^{-1}$ Mpc) at low and high redshifts ($0.05 \leqslant z \leqslant 0.83$) were used to determine the linear amplitude of mass fluctuations and the non-relativistic matter density in a Universe with a cosmological constant (Bahcall & Fan 1998; Bahcall & Bode 2003). Recently, these data have been used to put constraints on some of the free parameters of the standard cosmological model and to investigate the possibility that dark energy evolves in time, instead of being constant (Campanelli et al. 2012). Also, Devi et al. (2013) constrained different dark energy models by using the number count data of massive clusters in the context of the SCM. Their results show that the cluster number density for different dark energy models significantly deviates from that obtained in the concordance ΛCDM Universe, especially at high redshifts. Furthermore, in scalar field DE models, Devi et al. (2013) showed that the tachyon scalar field with a linear potential has the largest deviations from the ΛCDM model.

In this work, in the context of the extended SCM in the presence of shear and rotation (hereafter, ESCM), using the number count data of massive galaxy clusters, we put constraints on the parameter α related to the combined shear and rotation parameter in the equations dealing with the ESCM. To do this, we use the available number count data from massive X-ray clusters presented in Campanelli et al. (2012). Since we want to focus on studying the contribution of the shear and rotation term in massive clusters, we limit ourselves to a standard ΛCDM cosmology. Moreover, we adopt the Navarro-Frenk-White (NFW) profile for the virialized halo mass density as found in N-body simulations (Navarro et al. 1997).

The paper is organised as following. In section 2, we present the ESCM and study the spherical collapse parameters in the presence of shear and rotation. In section 3, we describe how to evaluate the number counts of massive clusters and in section 4 we constrain the cosmological parameters including the shear and rotation parameter by applying a Markov Chain Monte Carlo (MCMC) analysis, using SnIa, BAO, CMB, the Hubble parameter, the Big Bang Nucleosynthesis (BBN) and the number count data of massive clusters. Our results and conclusion are presented in section 5.

2 EXTENDED SPHERICAL COLLAPSE MODEL

In this section, we review the derivation of the differential equations determining the evolution of matter overdensity δ, using the spherical collapse model in the presence of shear and rotation. The spherical collapse model in dark energy cosmologies was investigated in detail in Pace et al. (2010), based on the work of Abramo et al. (2007). Pace et al. (2010) extended the evolution equation to general geometries and cosmologies, so that their results may be applied to models beyond the ΛCDM model. The effects of shear and rotation on the evolution of matter overdensities were investigated in homogeneous DE cosmologies (Del Popolo et al. 2013a,c,b) and in clustering DE cosmologies (Pace et al. 2014b). Using the non-linear differential equations for the evolution of the matter density contrast derived from Newtonian hydrodynamics in Pace et al. (2010), Del Popolo et al. (2013c) showed that the parameters of the spherical collapse model become mass dependent. Due to the stronger effect of rotation with respect to shear, the linear overdensity parameter δ_c is enhanced with respect to the standard case, therefore the collapse is slowed down and less objects will form in general. A similar effect was also obtained for the virial overdensity parameter Δ_V (Del Popolo et al. 2013c). On the other hand, in the high mass tail of the mass function, they showed that the effects of shear and rotation are very small, not influencing in an appreciable way the number of objects at high mass.

The equations describing the evolution of the density contrast $\delta_j \equiv \delta\rho_j/\bar{\rho}_j$ and of the peculiar velocity $\vec{u}_j$, together with the Poisson equation for the peculiar potential ϕ are (Pace et al. 2010; Batista & Pace 2013; Pace et al. 2014b),

$$\dot{\delta}_{\rm j} + 3H(c^2_{{\rm eff},j} - \bar{w}_{\rm j})\delta_{\rm j} + [1+\bar{w}_{\rm j} + (1+c^2_{{\rm eff},j})\delta_j]\vec{\nabla}\cdot\vec{u}_{\rm j} = 0\,, \tag{1}$$

$$\dot{\vec{u}}_{\rm j} + 2H\vec{u}_{\rm j} + (\vec{u}_{\rm j}\cdot\vec{\nabla}\vec{u}_{\rm j}) + \frac{1}{a^2}\vec{\nabla}\phi = 0\,, \tag{2}$$

$$\nabla^2\phi - 4\pi G a^2\sum_{\rm k}\rho_{\rm k}\delta_{\rm k}(1+3c^2_{{\rm eff},k}) = 0\,, \tag{3}$$

where we already took into account the top-hat density profile for the density perturbation ($\vec{\nabla}\delta_j = 0$) and we worked in comoving coordinates ($\vec{x}$), $\vec{\nabla} \equiv \vec{\nabla}_{\vec{x}}$. In the previous set of equations, $\bar{w}_{\rm j} = \bar{P}_{\rm j}/(\bar{\rho}_{\rm j}c^2)$ is the background equation-of-state parameter of the fluid and $c^2_{\rm eff,j} = \delta P_{\rm j}/(c^2\delta\rho_{\rm j})$ is the effective sound speed of perturbations in units of the speed of light.

Shear and rotation enter in the picture by taking the divergence of equation 2, since we are interested in the evolution of the divergence of the peculiar velocity $\theta \equiv \vec{\nabla}\cdot\vec{u}$

$$\dot{\theta} + 2H\theta + \frac{1}{3}\theta^2 + \sigma^2 - \omega^2 + \frac{1}{a^2}\vec{\nabla}^2\phi = 0\,, \tag{4}$$

where $\sigma^2 = \sigma_{ij}\sigma^{ij}$ is the shear tensor and $\omega^2 = \omega_{ij}\omega^{ij}$ the rotation tensor and are defined as

$$\sigma_{ij} = \frac{1}{2}\left(\frac{\partial u^j}{\partial x^i} + \frac{\partial u^i}{\partial x^j}\right) - \frac{1}{3}\theta\delta_{ij}\,, \tag{5}$$

$$\omega_{ij} = \frac{1}{2}\left(\frac{\partial u^j}{\partial x^i} - \frac{\partial u^i}{\partial x^j}\right)\,, \tag{6}$$

To obtain equation 4, we used the following relation

$$\nabla\cdot[(\vec{u}\cdot\nabla)\vec{u}] = \frac{1}{3}\theta^2 + \sigma^2 - \omega^2\,. \tag{7}$$

Following Fosalba & Gaztanaga (1998a,b); Gaztanaga & Fosalba (1998); Engineer et al. (2000), it is possible to relate the evolution of δ to the evolution of the radius R of the overdensity

$$\frac{d^2R}{dt^2} = \frac{4}{3}\pi G\rho R - (\sigma^2-\omega^2)\frac{R}{3} + \frac{\Lambda}{3}R = -\frac{GM}{R^2} - (\sigma^2-\omega^2)\frac{R}{3} + \frac{\Lambda}{3}R\,, \tag{8}$$

similar to the equation of the spherical collapse model taking into account the angular momentum (Peebles 1993; Nusser 2001;

Zukin & Bertschinger 2010b,a)

$$\frac{d^2R}{dt^2} = -\frac{GM}{R^2} + \frac{L^2}{M^2R^3} + \frac{\Lambda}{3}R = -\frac{GM}{R^2} + \frac{4}{25}\Omega^2 R + \frac{\Lambda}{3}R\,, \tag{9}$$

where we used the momentum of inertia of a sphere, $I = 2/5MR^2$. The last equation shows a close connection between the vorticity ω and the angular velocity Ω.

Considering the ratio of the rotational and gravitational terms, we get

$$\alpha = \frac{L^2}{M^3RG}\,. \tag{10}$$

Following the same argument for the rotation we obtain

$$\frac{\sigma^2 - \omega^2}{H^2} = -\frac{3}{2}\alpha \sum_k \Omega_{k,0} g_k(a)(1 + 3c^2_{\mathrm{eff},k})\delta_k\,, \tag{11}$$

where $g_k(a)$ represents the time evolution of the fluid k and we assumed that all the fluids are affected by shear and rotation in the same way.

The effects of shear and rotation on δ can be obtained by solving equations 1, 2 and 3, together with equation 11.

Specialising to the standard ΛCDM model where only matter is clustering ($\bar{w}_\mathrm{m} = c^2_{\mathrm{eff},\,\mathrm{m}} = 0$), the equation of motion for the overdensity δ_m becomes

$$\delta_\mathrm{m}'' + \left(\frac{3}{a} + \frac{E'}{E}\right)\delta_\mathrm{m}' - \frac{4}{3}\frac{\delta_\mathrm{m}'^2}{1+\delta_\mathrm{m}} - \frac{3}{2a^5E^2}(1-\alpha)\Omega_{\mathrm{m},0}\delta_\mathrm{m}(1+\delta_\mathrm{m}) = 0\,, \tag{12}$$

where E represents the time evolution of the Hubble function, $H(a) = H_0E(a)$ and is given by

$$E^2(a) = \frac{\Omega_{\mathrm{m},0}}{a^3} + \Omega_\Lambda\,. \tag{13}$$

Shear and rotation are non-linear quantities and will not affect the evolution of perturbations at the linear level. Therefore the evolution of matter perturbations in the linear regime is the standard growth factor equation

$$\delta_\mathrm{m}'' + \left(\frac{3}{a} + \frac{E'}{E}\right)\delta_\mathrm{m}' - \frac{3}{2a^5E^2}\Omega_{\mathrm{m},0}\delta_\mathrm{m} = 0\,. \tag{14}$$

2.1 Determination of δ_c and Δ_vir in the ESCM

It is well known that the linear overdensity δ_c and the virial overdensity Δ_vir are two important quantities characterising the scenario of the SCM. Moreover, the first quantity is crucial in the Press-Schechter formalism (Press & Schechter 1974; Bond et al. 1991; Sheth & Tormen 2002) and the latter determines the size of virialised structures. Here we calculate these two quantities in the context of the ESCM and study how shear and rotation can affect them. To this end, we follow the general approach presented in Pace et al. (2010, 2012, 2014b,a) to calculate the linear overdensity δ_c and virial overdensity Δ_vir and we refer to these works for a more detailed description.

Since equation (12) is a non-linear equation, the value of δ_m diverges at some characteristic redshift called the collapse redshift z_c. Numerically, the divergence is achieved when δ_m exceeds the value 10^7 (this value is the minimum one necessary to have a solution numerically stable and independent of this value). The linear overdensity δ_c is the value of the overdensity at collapse redshift $\delta_\mathrm{m}(z_\mathrm{c})$ obtained by solving the linearised equation (14) with the same initial conditions applied to the non-linear equation (12).

In the left panel of Fig. (1), we plot the linear overdensity parameter at the present time, $\delta_\mathrm{c}(z=0)$, as a function of the parameter α. In the case of $\alpha = 0$, the linear overdensity δ_c is ≈ 1.675, as expected in a ΛCDM cosmology with $\Omega_{\mathrm{m},0} = 0.3$. By increasing α, the value of δ_c increases accordingly. Since in the presence of shear and rotation the collapse is delayed by their mutual interplay, we need a higher value for the initial overdensity to reach the collapse and this translates into a higher value of δ_c.

Another important quantity in the SCM is the virial overdensity, defined as the overdensity with respect to the background (or critical) density at the time of virialization. Note that this aspect is not native into the formalism and has to be introduced in it. This quantity is defined as $\Delta_\mathrm{vir} = \zeta(x/y)^3$, where ζ is the overdensity at the turn-around redshift, x is the scale factor divided by the turn-around scale factor and y is the ratio between the virialised radius and the turn-around radius (Wang & Steinhardt 1998; Wang 2006). In an Einstein-de Sitter (EdS) Universe, it is easy to show that $y = 1/2$, $\zeta \simeq 5.5$ and $\Delta_\mathrm{vir} \simeq 178$ at any time. However, in a ΛCDM universe, Δ_vir is affected by the presence of the cosmological constant and the virial overdensity changes as a function of time.

In the right panel of Fig. (1), we show the evolution of the virial overdensity with respect to the background density computed at the present time, $\Delta_\mathrm{vir}(z=0)$, as a function of α for a ΛCDM cosmology within the framework of the ESCM. Dark energy opposes to gravity and prevents the collapse of structures. In the EdS model, this value is constant, but for the ΛCDM model and dark energy models in general, this is not the case any more. In particular, for a ΛCDM cosmology the value of Δ_vir in standard SCM is roughly 260 times the background density. In addition, in the ESCM due to the inclusion of the shear and rotation term, we see that Δ_vir increases by increasing the parameter α. This result is similar to what found for the linear overdensity δ_c in the ESCM. We note that the SCM parameters δ_c and Δ_vir become mass dependent in the presence of shear and rotation as indicated in Del Popolo et al. (2013a,c,b). In fact the effect of the parameter α on the SCM parameters can be easily seen from equation (12). Since the non-linear quantity α depends on mass, we expect that in general the SCM parameters are mass-dependent and change for different mass scales. In the next section, we provide a phenomenological expression representing the variation of α in terms of the mass and show how the mass function and the number counts of massive galaxy clusters depend on α.

Since one of the main ingredients in our analysis is the virial overdensity Δ_vir, it is important to discuss a bit more in detail this issue. While it is straightforward to evaluate the virial overdensity in an EdS model where only the dark matter component is present, this is not true for more complicated models where also an additional fluid, either in the form of a cosmological constant Λ or a more general dark energy component, is present. The main problem to face is the role of this additional component to the virialization process, not to mention further complications when the dark energy component clusters as well. Several authors have proposed different recipes to take this into account and results could differ sensibly between each other. Wang & Steinhardt (1998); Lokas (2001); Basilakos (2003); Horellou & Berge (2005); Wang (2006); Basilakos & Voglis (2007) have studied the virialization process on smooth dark energy models and Bartelmann et al. (2006) have extended the formalism to early dark energy models (but see also Pace et al. 2010); Maor & Lahav (2005) and Nunes & Mota (2006) instead investigated the virialization process when dark energy possesses fluctuations. Finally, Basilakos et al. (2010) evaluated the

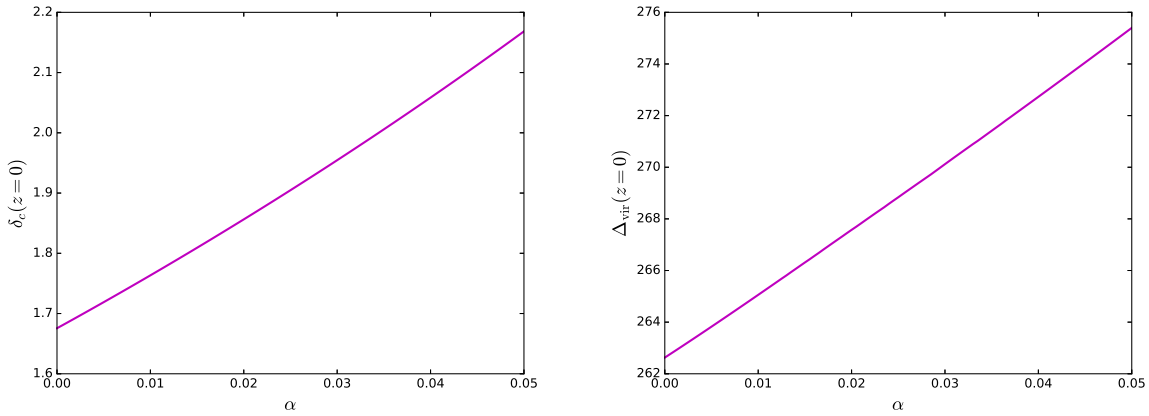

Figure 1. *Left* (*right*) *panel*: Variation of the linear overdensity (virial overdensity with respect to the background density) at the present time $\delta_c(z=0)$ ($\Delta_{vir}(z=0)$) in terms of the parameter α in a ΛCDM universe.

mass function of cluster-size halos and their redshift distribution for different cosmological models and confronted to the predictions of the concordance ΛCDM model finding that the predictions of eight models were statistically different from the ones of the ΛCDM model.

This discussion clearly shows that a general consensus on the subject is still lacking and more importantly, that our discussion could be severely affected by the choice of the prescription to evaluate the virial overdensity and hence the size of cluster. We therefore decided to use the prescription to evaluate Δ_{vir} of Wang & Steinhardt (1998) and Maor & Lahav (2005) which are in agreement with a fully general relativistically analysis performed by Meyer et al. (2012).

3 MASSIVE GALAXY CLUSTER NUMBER COUNT

In this section we investigate the mass function and the number counts of massive galaxy clusters in the framework of the ESCM formalism and study how shear and rotation affect observable quantities related to galaxy clusters number counts.

3.1 Mass function and number of clusters

Galaxies and cluster of galaxies are embedded in the extended cold dark (CDM) matter haloes. In the Press-Schechter formalism, the abundance of CDM haloes in the Universe can be described in terms of their mass and a Gaussian distribution function (Press & Schechter 1974). In fact, the fraction of the volume of the Universe which collapses into an object of mass M at a characteristic redshift z is expressed by a Gaussian distribution function. In the Press-Schechter formalism, the comoving number density of collapsed objects with masses in the range of M and $M+dM$ at the cosmic redshift z can be written as (Press & Schechter 1974; Bond et al. 1991):

$$\frac{dn(M,z)}{dM} = \frac{\bar{\rho}_0}{M}\frac{d\nu(M,z)}{dM} f(\nu)\,, \tag{15}$$

where $\bar{\rho}_0$ is the background density at the present time, and

$$\nu(M,z) = \frac{\delta_c}{\sigma}\,, \tag{16}$$

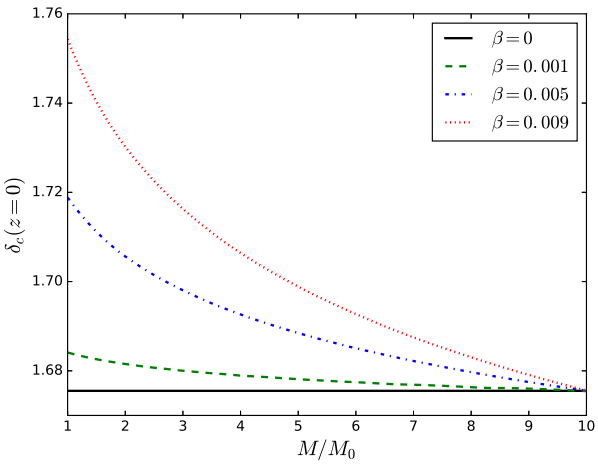

Figure 2. The present time value of the linear overdensity $\delta_c(z=0)$ as a function of mass computed for different values of the slope parameter β. The black solid line shows results for $\beta=0$ (the standard spherically symmetric case), the green dashed curve the model with $\beta=0.001$, while the blue dot-dashed and the red dotted line show results for $\beta=0.005$ and $\beta=0.009$, respectively. The normalization mass M_0 is defined as $M_0 = 8\times10^{14}\,h^{-1}\,M_\odot$.

where σ is the r.m.s. of the mass fluctuations in spheres of mass M and $f(\nu)$ is the mass function. The standard mass function presented by Press & Schechter (1974) differs from simulations at both high and low mass haloes (Sheth & Tormen 1999, 2002). Therefore we will use the following mass function formula proposed by Sheth & Tormen (1999, 2002), the so called ST mass function

$$f(\nu) = 0.2709\sqrt{\frac{2}{\pi}}\left(1+1.1096\nu^{0.3}\right)\exp\left(-\frac{0.707\nu^2}{2}\right). \tag{17}$$

The predictions of N-body simulations show that the abundance of clusters is well described by ST mass function up to $z\sim2$ (Jenkins et al. 2001). For higher redshifts, Jenkins et al. (2001) showed deviations between the predictions of N-body simulations and the ST mass function. By using high-resolution N-body

simulations, Reed et al. (2003) predicted a fewer numbers of haloes than the ST mass function at $z \sim 15$. However, several other works showed that already beyond $z \gtrsim 2$, when using high resolution N-body simulations, the ST mass function is not a good fit (see e.g., Klypin et al. 2011). Here, nevertheless, this is not a big issue since our cluster sample spans a limited redshift range and in any case this is $z \lesssim 1$. To show how the results depends on the choice of the mass function, we compute the number of haloes in the redshift range $0 \leqslant z \leqslant 1$ by using the prescription of Reed et al. (2007) and the ST mass function. Our results show a difference less than 1% for mass scales $1 \times 10^{13} h^{-1} M\odot$, approximately 4% for mass scales $5 \times 10^{13} h^{-1} M\odot$ and roughly 11% for mass scales $5 \times 10^{14} h^{-1} M\odot$. For higher mass scales the difference may be as large as 20% but these high mass clusters are very rare and can not affect our results. Notice that these results are in agreement with the results of Jenkins et al. (2001).

In a Gaussian density field, the amplitude of mass fluctuations σ is given by

$$\sigma^2(R,z) = \frac{1}{2\pi^2} \int_0^\infty k^2 P(k,z) W^2(kR) dk \,, \tag{18}$$

where R is the comoving radius of the spherical overdense region, $W(kR)$ is the Fourier transform of a spherical top-hat filter and $P(k,z)$ is the linear matter power spectrum of density fluctuations at redshift z (Peebles 1993). The linear matter power spectrum at redshift z can be written as

$$P(k,z) = P_0(k) T^2(k) D^2(z) \,, \tag{19}$$

where we adopted the simple power law formula for P_0 as $P_0(k) = A k_s^n$ with the nearly scale-invariant spectrum corresponding to $n_s = 0.96$. We also adopted the transfer function $T(k)$ which considers baryonic features and was introduced in Eisenstein & Hu (1998).

The comoving number density of clusters above a certain mass M_0 at collapse redshift z is

$$n(>M_0,z) = \int_{M_0}^\infty \frac{dn(M',z)}{dM'} dM' \,. \tag{20}$$

The comoving number of clusters per unit redshift with mass greater than a fiducial mass value M_0 is given by

$$N_{\rm bin} = n(M > M_0, z) \frac{dV}{dz} \,, \tag{21}$$

where

$$V(z) = 4\pi \int_0^z \frac{d_{\rm L}^2(z')}{(1+z')^2 H(z')} dz' \,, \tag{22}$$

is the comoving volume at redshift z, and

$$d_{\rm L}(z) = (1+z) \int_0^z \frac{dz'}{H(z')} \,, \tag{23}$$

is the luminosity distance. It should be noted that the comoving volume depends on the cosmological model and hence volume effects will be introduced in the determination of the number counts. In the next section we will present the observational data on the abundance of massive galaxy clusters with masses above $M_0 = 8 \times 10^{14}\ h^{-1}\ M_\odot$ within a comoving radius of $R_0 = 1.5\ h^{-1}\ Mpc$ at redshift $0.05 \leqslant z \leqslant 0.83$. In this section we calculate the number of massive clusters $N_{\rm bin}$ with masses above M_0 as a function of redshift to investigate how shear and rotation can affect the number of clusters. We also compute the total number count of massive clusters above a given mass M_0 at the present time $z = 0$ up to cosmic redshift z as

$$N = \int_0^z N_{\rm bin} dz' = \int_0^z n(M > M_0, z') \frac{dV}{dz'} dz' \,. \tag{24}$$

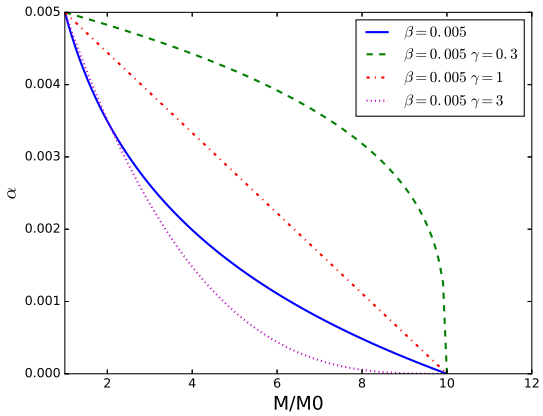

Figure 3. Logarithmic and power-law parametrizations for α as a function of mass scale M/M_0. The blue-solid, green-dashed, red-dotted-dashed and purple-dotted curves, represent the logarithmic, power-law with $\gamma = 0.3$, $\gamma = 1$ and $\gamma = 3$ parametrizations, respectively.

Since there is not a theoretical expression describing the variation of α in terms of mass, we examine a logarithmic relation

$$\alpha = -\beta \log_{10} \frac{M}{M_s} \,, \tag{25}$$

where M_s is a normalization mass and β is a constant parameter representing the slope of the parameter α. In what follows we set $M_s = 10 M_0 = 8 \times 10^{15} h^{-1} M_\odot$. Objects of such high mass are very rare, therefore we do not expect our analysis to be affected by this value. This is further justified by the fact that the abundance of massive cluster with $M > M_0$ is a factor of 10^6 larger than clusters with $M > 10 M_0$. Notice that Eq. (25) is a phenomenological relation and one can consider other possibilities such as a power-law parametrization

$$\alpha = \beta \frac{\left(1 - \frac{M}{M_s}\right)^\gamma}{0.9^\gamma} \,, \tag{26}$$

where the denominator is chosen to achieve the same value of α for the two different logarithmic and power-law parametrizations at M_0. In Fig (3) we show the evolution of α as a function of mass scale M/M_0 for both the logarithmic and the power-law parametrization. In all cases, we set the slope parameter as $\beta = 0.005$ and examine different values of γ for the power-law parametrization: 0.3, 1.0 and 3.0. We see that both models have the same value $\alpha = 0.005$ at mass scale $M = M_0$ and $\alpha = 0$ for $M > 10 M_0$. Quantitatively speaking, in order to distinguish how the results may be changed for different parametrizations, we compute the number of massive clusters with mass scale $M > M_0$ in the redshift range $0 < z < 1$ using the ST mass function. We found that the differences between the logarithmic and the power-law parametrization are of the order of 0.1%, 0.5% and 1.5%, respectively, for $\gamma = 3$, $\gamma = 1$ and $\gamma = 0.3$. We see that such small differences would not affect our results. Since the logarithmic relation is defined with one parameter (β) to describe the mass dependency of α, in what follows we adopt this parametrization and continue our analysis on the basis of Eq. (25).

As mentioned above, the linear overdensity δ_c is a crucial parameter in the Press-Schechter formalism and in Fig. (2) we show how the present time value of δ_c varies with mass for three different values of β with respect to the standard case with $\beta = 0$. Increasing β increases α which results into a higher value for the critical linear

overdensity. In the case of $M = 10M_0$, we see that for all models δ_c tends to the fiducial value 1.675 representing the standard ΛCDM value without shear and rotation. Note that in this case we set $\Omega_m = 0.3$.

In the left panel of Fig. (4) we show the number counts of massive clusters, N_{bin}, above a given mass M_0 as a function of redshift z for different values of the slope parameter β as indicated in the legend. It can be seen that for higher values of β we find less massive objects, in agreement with the general discussion above.

In the right panel of Fig. (4) we show the total number counts of massive clusters, N, in terms of the cosmic redshift for different values of the parameter β as described in the legend. In analogy with what found for the number counts, we see that for higher values of β massive galaxy clusters are less abundant. We also see that for $z \gtrsim 1$ we reach a plateau in the total number of clusters above a given mass M_0. This is due to the fact that such massive objects are not yet formed above $z \gtrsim 1$.

4 OBSERVATIONAL CONSTRAINTS ON THE β PARAMETER

To constrain β from observational data, we perform a likelihood analysis with current available observational data. After introducing the observational data used in this work, we will present and discuss the results. Since shear and rotation only affect the non-linear evolution of structures, to constrain β we use the data related to number counts of massive galaxy clusters in different redshift bins as introduced in Campanelli et al. (2012). Although a direct mass measurement is a difficult task, Campanelli et al. (2012) used a simple mass-temperature relation to estimate the number counts of massive galaxy clusters in four redshift bins with mass greater than $M_0 = 8 \times 10^{14} h^{-1} M_\odot$. We use the most recent geometrical probes like SNIa, cosmic microwave background (CMB) and baryon acoustic oscillation (BAO) to fix the geometry and add the data of massive galaxy clusters number count to find the best value of the slope β. Finally, since the relations in the non-linear regime we use to convert masses are well tested in simulations in ΛCDM models only, we restrict ourself to this cosmology.

We use the SnIa data from the Union 2.1 sample (Suzuki et al. 2012) which includes 580 SnIa over the redshift range $0 < z < 1.4$. The χ^2_{sn} is

$$\chi^2_{sn} = \mathbf{X}^T_{sn} \mathbf{C}^{-1}_{sn} \mathbf{X}_{sn} \,, \tag{27}$$

where $\mathbf{X}_{sn} = \mu_{th} - \mu_{ob}$, $\mu_{th}(z) = 5 \log_{10} \left[(1+z) \int_0^z \frac{dx}{E(x)} \right] + \mu_0$ and μ_{ob} is the observational value of the distance module. For $\mathbf{C}^{-1}_{sn}$ we use the covariance matrix including systematic uncertainties from Suzuki et al. (2012). Note that in this case the results are marginalized over the noisy parameter μ_0 so that the result does not depend on it.

For BAO, the χ^2_{bao} is given by

$$\chi^2_{bao} = \mathbf{Y}^T \mathbf{C}^{-1}_{bao} \mathbf{Y} \,, \tag{28}$$

where $\mathbf{Y} = (d(0.1) - d_1, \frac{1}{d(0.35)} - \frac{1}{d_2}, \frac{1}{d(0.57)} - \frac{1}{d_3}, d(0.44) - d_4, d(0.6) - d_5, d(0.73) - d_6)$. The quantity $d(z)$ is defined through

$$d(z) = \frac{r_s(z_{drag})}{D_V(z)} \,, \tag{29}$$

where $r_s(z_{drag})$ is the comoving sound horizon at the drag epoch, namely the time when the baryons are "released" from the drag of the photons, and $D_V(z)$ is a combination of the angular diameter distance and expansion rate of the Universe $H(z)$

$$D_V(z) = \left[(1+z)^2 D_A^2(z) \frac{z}{H(z)} \right]^{\frac{1}{3}} \,. \tag{30}$$

We use the fitting formula for the redshift of the drag epoch, z_{drag}, given in Eisenstein & Hu (1998) and the covariance matrix $\mathbf{C}^{-1}_{bao}$ introduced in Hinshaw et al. (2013). The observational data for d_i are presented in Tab. (1).

Table 1. BAO data and their references.

z	d_i	Survey	References
0.106	0.336	6dF	Beutler et al. (2011)
0.35	0.113	SDSS-DR7	Padmanabhan et al. (2012)
0.57	0.073	SDSS-DR9	Anderson et al. (2013)
0.44	0.0916	WiggleZ	Blake et al. (2011)
0.6	0.0726	WiggleZ	Blake et al. (2011)
0.73	0.0592	WiggleZ	Blake et al. (2011)

CMB data can also be described through a covariance matrix $\mathbf{C}^{-1}_{cmb}$,

$$\chi^2_{cmb} = \mathbf{X}^T_{cmb} \mathbf{C}^{-1}_{cmb} \mathbf{X}_{cmb} \,, \tag{31}$$

where

$$\mathbf{X}_{cmb} = \begin{pmatrix} R - R^{pl} \\ l_a - l_a^{pl} \\ \Omega_b h^2 - (\Omega_b h^2)^{pl} \end{pmatrix} \,, \tag{32}$$

and the superscript "pl" refers to the Planck value and the quantities l_a and R are defined as

$$l_a = \pi \frac{D_A(z_*)}{r_s(z_*)} \,, \quad R = \sqrt{\Omega_m} H_0 D_A(z_*) \,.$$

For z_* (last scattering redshift), we use the fitting formula from Hu & Sugiyama (1996) and the covariance matrix from the analysis of Huang et al. (2015).

To obtain the number counts of massive galaxy clusters in different redshift bins from a theoretical point of view, we follow the same procedure presented in Campanelli et al. (2012). The redshift bins and the effective fraction of the observed comoving volume, f_{sky}, are summarized in Tab. (2). Data in bin 1 are extracted from a sample of 61 clusters introduced in Ikebe et al. (2002). The X-ray temperatures and fluxes of the cluster sample are measured with ASCA and ROSAT satellites. These clusters form a flux-limited complete sample in the redshift range $0 < z < 0.1$ and the effective fraction of observed comoving volume in this case is 0.309. The data in bin 2 are extracted from 14 massive clusters which are both redshift- and flux-limited Henry (2000). The average redshift of these clusters is 0.38 and cover a fraction of 0.012 of the observed comoving volume. In Bahcall & Fan (1998); Bahcall & Bode (2003) the most massive clusters of galaxies at redshifts $z > 0.5$ have been studied and used to constrain the cosmological parameters Ω_m and σ_8. In bin 3 we use the data of massive clusters in the redshift range $0.5 < z < 0.65$ with a tiny fraction of observed volume. To see the complete list of cluster data used here, we refer to (Campanelli et al. 2012). Note that since these data come from observational surveys which trace a specified portion of sky, we are not able to change these redshift bins in our analysis.

Due to the low number of clusters in each bin, the Poisson

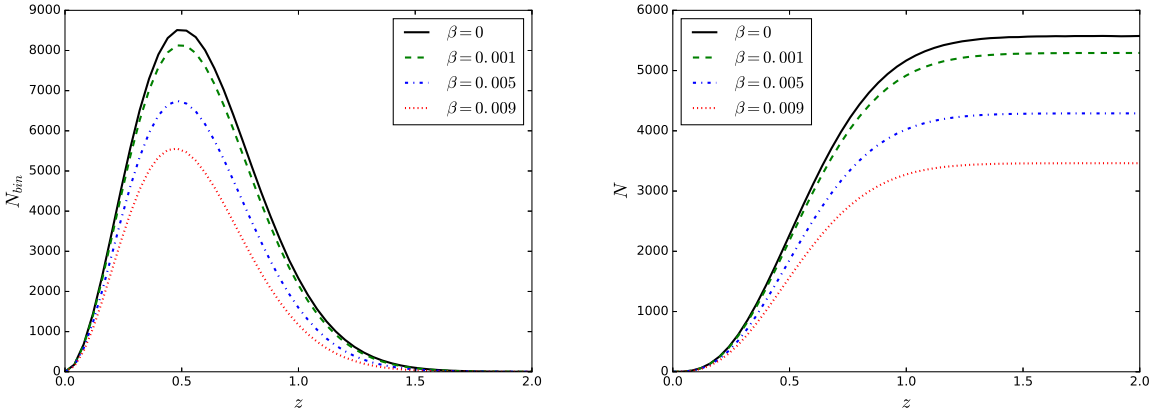

Figure 4. *Left* (*right*) *panel*: Evolution of the number counts (total number counts) of massive clusters as a function of the cosmic redshift for objects with masses above $M_0 = 8 \times 10^{14} h^{-1} M_\odot$ and for different values of the slope parameter β computed in the ΛCDM cosmology. Line styles and colours are as in Fig. (2).

Table 2. Redshift intervals for the number count data of massive galaxy clusters. $f_{\rm sky}(i)$ represents the effective fraction of the observed comoving volume of the $i^{\rm th}$ bin.

bin i	$z_1^{(i)}$	$z_2^{(i)}$	$z_c^{(i)}$	Ref.	$f_{\rm sky}(i)$
1	0.00	0.10	0.050	Ikebe et al. (2002)	0.309
2	0.30	0.50	0.375	Henry (2000)	0.012
3	0.50	0.65	0.550	Bahcall & Fan (1998); Bahcall & Bode (2003)	0.006
4	0.65	0.90	0.825	Donahue et al. (1998)	0.001

statistics is used to define the likelihood function. Therefore the $\chi^2_{\rm num}$, taking into account the uncertainty in the comoving number of clusters, $\Delta N_{{\rm obs},i}$, is (see Campanelli et al. 2012, for details)

$$\chi^2_{\rm num} = 2 \sum_{i=1}^{4} \left[N_i - N'_{{\rm obs},i} \left(1 + \ln N_i - \ln N'_{{\rm obs},i} \right) \right] + \xi^2 \ , \qquad (33)$$

where $N'_{{\rm obs},i} = N_{{\rm obs},i} + \xi \Delta N_{{\rm obs},i}$ and $N_{{\rm obs},i}$ is the number of clusters in each bin and is defined as

$$N_{{\rm obs},i} = f_{\rm sky}^{(i)} \int_{z_1^{(i)}}^{z_2^{(i)}} \int_{g(M_0)}^{\infty} \frac{dn(M',z')}{dM'} dM' \frac{dV}{dz'} dz' \ , \qquad (34)$$

where $g(M_0)$ relates the observed mass to the virial mass which depends on the model and the parameters. Note that due to the asymmetric errors in X-ray temperature of clusters, the errors for the number of clusters in each bin $\Delta N_{{\rm obs},i}$ will also be asymmetric. For the mass-concentration relation, we use the prescription of Prada et al. (2012). We use the procedure introduced in appendix B of Campanelli et al. (2012) to find $g(M_0)$. In equation (33), ξ is a uni-variate Gaussian random variable which is introduced to consider the uncertainty on the number of clusters in each bin. The values of $N_{{\rm obs},i}$ and $\Delta N_{{\rm obs},i}$ are shown in Tab. 3.

Note that since the mass-temperature relation needs the virial overdensity with respect to the critical density, in the first column of Tab. (3) we show the value of the virial overdensity $\Delta'_{\rm vir}$ defined as

$$\Delta'_{\rm vir} = \frac{\Omega_{\rm m,0}(1+z)^3}{E^2(z)} \Delta_{\rm vir} \ , \qquad (35)$$

where $\Delta'_{\rm vir}$ and $\Delta_{\rm vir}$ are the virial overdensity with respect to the critical and the background matter density, respectively. In the model considered here, $\Delta_{\rm vir}$ depends also on the mass as for the critical overdensity contrast. Since the virial overdensity in the range of mass $(M_0, 10M_0)$ is practically constant [1], we evaluate the virial overdensity for M_0 neglecting its mass evolution to compare with observations in Tab. (3).

The overall likelihood function for all data sets used is

$$\mathcal{L}_{\rm tot} = \mathcal{L}_{\rm sn} \times \mathcal{L}_{\rm bao} \times \mathcal{L}_{\rm cmb} \times \mathcal{L}_{\rm num} \ , \qquad (36)$$

which leads to

$$\chi^2_{\rm tot} = \chi^2_{\rm sn} + \chi^2_{\rm bao} + \chi^2_{\rm cmb} + \chi^2_{num} \ . \qquad (37)$$

In our analysis, the free parameters are $P = \{\Omega_{\rm DM}, \Omega_{\rm b}, h, \beta, \xi\}$, where $\Omega_{\rm m} = \Omega_{\rm DM} + \Omega_{\rm b}$ is the total matter in the Universe. Other two relevant parameters ($n_{\rm s} = 0.9646$ and $\sigma_8 = 0.818$) are fixed to the Planck values (Planck Collaboration XIII 2015). Our purpose in this analysis is to put a constraint on the slope of shear and rotation parameter β appearing in the non-linear equations in the ESCM formalism by using the data for the number counts of massive galaxy clusters.

We perform a MCMC analysis to find the best fit values of the parameters as well as their uncertainties. In addition, our results are marginalized over ξ. To do so, we use the GetDist package [2] where for a large number of chains the package automatically marginalizes over a specific parameter. Results are summarized in Tab. (4).

In Fig. (5) we show the confidence regions for the ($\Omega_{\rm m}$, β) pair parameters. In particular, while β is constrained at the $1-\sigma$ confidence level, we find only an upper limit at the $2-\sigma$ and $3-\sigma$

[1] The virial overdensity varies about 0.2% for the mass range between $(M_0, 10M_0)$ and for the best fit parameters found in this work, its value is 268.6.

[2] https://github.com/cmbant/getdist

Table 3. Observational data for cluster number counts in different redshifts bins (Campanelli et al. 2012).

	bin 1 $[T_{X,0}(\mathrm{keV}), N_{\mathrm{obs},1}]$	bin 2 $[T_{X,0}(\mathrm{keV}), N_{\mathrm{obs},2}]$	bin 3 $[T_{X,0}(\mathrm{keV}), N_{\mathrm{obs},3}]$	bin 4 $[T_{X,0}(\mathrm{keV}), N_{\mathrm{obs},4}]$
$\Delta'_{\mathrm{vir}} \in [25, 175]$	$[7.37, 5^{+1}_{-0}]$	$[9.6, 0^{+0}_{-0}]$	$[10.9, 0^{+1}_{-0}]$	$[12.8, 0^{+1}_{-0}]$
$\Delta'_{\mathrm{vir}} \in]175, 375]$	$[6.15, 15^{+2}_{-4}]$	$[8.1, 1^{+0}_{-1}]$	$[9.1, 1^{+1}_{-0}]$	$[10.7, 1^{+0}_{-0}]$
$\Delta'_{\mathrm{vir}} \in]375, 750]$	$[5.54, 21^{+2}_{-5}]$	$[7.3, 1^{+4}_{-1}]$	$[8.2, 2^{+0}_{-1}]$	$[9.6, 1^{+0}_{-0}]$
$\Delta'_{\mathrm{vir}} \in]750, 1750]$	$[5.14, 24^{+1}_{-1}]$	$[6.7, 2^{+4}_{-1}]$	$[7.6, 2^{+0}_{-1}]$	$[8.9, 1^{+0}_{-0}]$
$\Delta'_{\mathrm{vir}} \in]1750, 3250]$	$[4.91, 24^{+2}_{-0}]$	$[6.4, 5^{+1}_{-3}]$	$[7.3, 2^{+0}_{-0}]$	$[8.5, 1^{+0}_{-0}]$

Table 4. The best value of parameters and $1-\sigma$, $2-\sigma$ and $3-\sigma$ uncertainty intervals.

Parameters	Best fit value	$1-\sigma$	$2-\sigma$	$3-\sigma$
Ω_{m}	0.284	± 0.0064	$^{+0.013}_{-0.012}$	$^{+0.017}_{-0.016}$
h	0.678	± 0.017	$^{+0.032}_{-0.033}$	$^{+0.038}_{-0.043}$
β	0.0019	$^{+0.0008}_{-0.0015}$	< 0.0043	< 0.0054

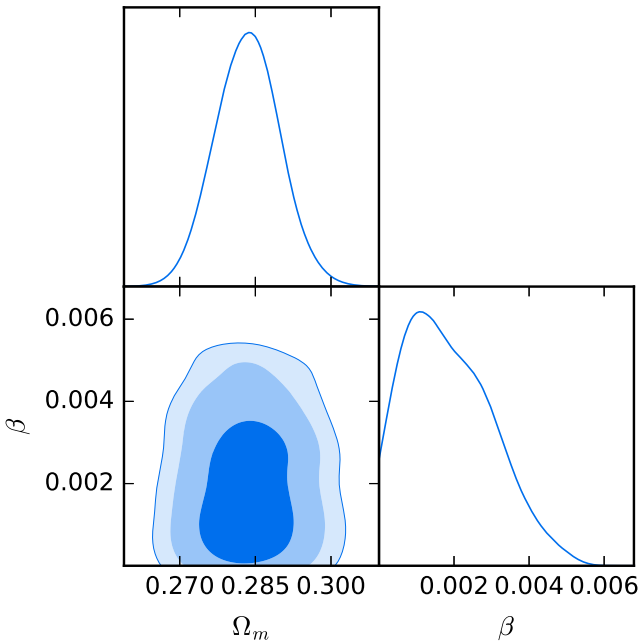

Figure 5. $1-\sigma$, $2-\sigma$ and $3-\sigma$ confidence regions for the (Ω_{m}, β) pair parameters.

confidence levels using massive clusters data. Since the posterior distribution for β includes also the null value with a relatively high amplitude and data quality is relatively poor, we are only able to get an upper limit for the 2- and the 3-σ confidence level. The best fit value of β is 0.0019 with a variance $^{+0.0008}_{-0.0015}$ at the $1-\sigma$ confidence level. Upper limits at the $2-\sigma$ and $3-\sigma$ confidence levels are shown in Tab. (4). Getting tighter constraints requires more accurate data of massive clusters.

Few works, as mentioned in the Introduction, have studied the effect of the term $\sigma^2 - \omega^2$ for the ΛCDM model, smooth and clustering dark energy models. More recently, Marciu (2016) applied the same formalism to warm dark matter models (obtained with a non-null equation of state for the dark matter component) in different dark energy clustering models. The author assumed a constant value for the additional non-linear term $\beta = 0.04$[3]

Our analysis allows us to compare the derived parameters Ω_{m} and h with recent work by the *Planck* team (Planck Collaboration XIII 2015). Using distance prior from TT, TE, EE and low P data, we find $h = 0.678 \pm 0.017$ at 1-σ level. This has to be compared with their value of $h = 0.6727 \pm 0.0066$ showing a good agreement between the two determination. Slightly different is the comparison with the total matter parameter Ω_{m}. Our finding is $\Omega_{\mathrm{m}} = 0.284 \pm 0.0064$ with respect to $\Omega_{\mathrm{m}} = 0.3089 \pm 0.0062$, showing an approximately $2-\sigma$ tension with the Planck result. This is easily explained by taking into account that we keep the normalization of the matter power spectrum fixed and the evolution of the halo mass function is modified by the presence of the α term in the equations of motion for matter perturbations. As explained before, the effect of the parameter α is to decrease the amount of structures formed. This implies that to fit the resulting mass function we require a lower matter density parameter Ω_{m} when σ_8 is held fixed. The Hubble parameter h is largely unaffected by this, since we determine it by using distance prior data.

Albeit small, a non-null value for β will have an appreciable effect of the cumulative mass function, as shown in detail in Fig. (6), where we compare, as a function of cosmic redshift z the comoving number density of objects above M_0 (top panel), the number of clusters in different redshift bins (middle panel) and the total number of clusters (bottom panel), respectively. We show results for the best fit value of β together with the $1-\sigma$ and $2-\sigma$ bound regions. For the sake of comparison we also show the standard mass function and derived quantities for the case of spherical symmetry ($\beta = 0$).

As expected, when $\beta \neq 0$, the number of cosmic objects formed is lower than in the standard case and the fact that differences are not negligible shows how much data need to improve, to have a reliable estimation of cosmological parameters based on cluster data. More quantitatively, the mass function at $z = 0$, evaluated with the best fit values of β, is roughly 20% smaller than that in the standard case with $\beta = 0$. This decrement, of the order of the uncertainty on the mass function itself, translates to a lower number of objects in each redshift bin (middle panel). The maximum value

[3] In Marciu (2016), their β corresponds to our α. which is valid for galactic scales. Note that in Marciu (2016), no scale dependence is assumed. Assuming our parametrization for α [Eq. (25)] and scales between $10^{11}\ h^{-1}M_{\odot}$ and $10^{11}\ h^{-1}M_{\odot}$, we find $\alpha \approx 0.01$ for $M \approx 10^{11}\ h^{-1}M_{\odot}$ and $\alpha = 7.4 \times 10^{-3}$ for $M \approx 10^{12}\ h^{-1}M_{\odot}$. This shows that the allowed value constrained by clusters would be a factor of four smaller than the one used by Marciu (2016). This implies a weaker effect on structure formation with respect to what found in the work.

for this quantity takes place approximately at $z \sim 0.5$, showing that the peak of cluster abundance is reached at this epoch. It is interesting to see that this value is largely unaffected by the presence of shear and rotation terms. This is due to the fact that the parameter α only slows down structure formation, but it does not affect its physics. Differences are in this case more limited and are of the order of 9% around the peak. Another indication that only the total number of objects is affected comes from the bottom panel, where we present the total number of objects. Note that the distribution flattens, reaching a plateau, around $z \gtrsim 1$, since at higher redshifts massive objects are not formed yet. Differences between the spherically symmetric case and the extended one are about 8%.

It is also interesting to compare our results with similar works in literature. Remember though that in our analysis we do not allow the normalization of the matter power spectrum to change. Campanelli et al. (2012), using only cluster data, found $\Omega_{\rm m} \geqslant 0.38$ and at the same time $\sigma_8 \leqslant 0.69$ at the $1-\sigma$ confidence level. Both results are in tension with our determination. This can be explained by the fact that we used cluster data with recent background data to constrain our model and the geometry being fixed in our analyses. Note that results of Campanelli et al. (2012), by considering the background data, are in well agreement with our results. On the other hand Mantz et al. (2010), using a constant dark energy model, find $\Omega_m = 0.23 \pm 0.04$ and $\sigma_8 = 0.82 \pm 0.05$ which are compatible with our results. In addition, our results are in complete agreement already at the $1-\sigma$ confidence level with Vikhlinin et al. (2009b) and Schuecker et al. (2003) which are in good agreement with results of Campanelli et al. (2012). Finally, it is worth to mention that these same data were used also by Bahcall & Fan (1998) and Bahcall & Bode (2003) who found low values for the matter density parameter ($\Omega_{\rm m} = 0.17 \pm 0.05$) and high normalization ($\sigma_8 = 0.98 \pm 0.10$). These results are both in disagreement with the ones found by Campanelli et al. (2012) and in this work. This shows how a different treatment of the data and different data set will lead to different results.

5 CONCLUSION

Massive galaxy clusters, being at the high mass end of the mass function are becoming a common tool in cosmology. Their abundance is a strong indicator of non-linear structure formation and it depends on the value of important cosmological parameters, such as the matter density parameter $\Omega_{\rm m}$, the mater power spectrum normalization σ_8 and the dark energy equation of state $w_{\rm de}$. A precise determination of the mass function is a current goal of both theoretical and observational studies, due to the wealth of implications related to it.

From a theoretical point of view, the mass function is related to the function $\delta_{\rm c}$, that, in the framework of the spherical collapse model, represents the density above which structures can form. In the standard approach, perturbations are assumed to be spherical and non rotating, but in an era of precision cosmology it is necessary to relax this assumption. Shear and rotation can be added naturally into this formalism as shown recently by Del Popolo et al. (2013a,c); Pace et al. (2014b) and their combination is parametrized via the parameter α. This extension of the simple spherically symmetric model makes such that $\delta_{\rm c}$ is now a function of both mass and redshift, contrary to the standard case where it only depends on time. This implies that the mass function and hence the total number of objects that can be observed will strongly depend on the evolution with mass of the parameter α. Since theory, so far, does not constrain it, in this work we choose a particularly simple form: $\alpha = -\beta \log_{10} \frac{M}{M_s}$, where β is the slope of the logarithmic relation and $M_s = 8 \times 10^{15}\ h^{-1}\ M_\odot$ is a normalization mass. When $M = M_s$, deviation from sphericity are null and we recover the standard case.

The combined effect of shear and rotation, due to the dominance of the latter, implies a decreased number of objects with respect to the spherically symmetric case since structure formation is slowed down.

Using data on massive clusters by Campanelli et al. (2012) we constrain, for the first time to our knowledge, the value of the slope β and we infer its consequences on the number of massive objects. In our analysis we find $\Omega_{\rm m} = 0.284 \pm 0.0064$, $h = 0.678 \pm 0.017$ and $\beta = 0.0019^{+0.0008}_{-0.0015}$ at $1-\sigma$ level, when keeping $\sigma_8 = 0.818$ fixed and restricting our analysis to a flat ΛCDM model. The value for h is in complete agreement with Planck Collaboration XIII (2015) but we find a slight tension for the value of $\Omega_{\rm m}$. This is due to the fact that, when fixing the normalization of the matter power spectrum, a decrement in the mass function requires a lower $\Omega_{\rm m}$. This has as consequence a decrement of about 9% in the number of massive clusters.

Our result for $\Omega_{\rm m}$ is in agreement with results in Mantz et al. (2010); Schuecker et al. (2003); Vikhlinin et al. (2009b) which use massive clusters to constrain cosmological parameters. In addition our results are compatible with results of Campanelli et al. (2012) when they combine geometrical data to the massive clusters data. At the same time, using the same data, Campanelli et al. (2012) is in disagreement with Bahcall & Fan (1998) and Bahcall & Bode (2003) who found a very low (high) value for $\Omega_{\rm m}$ (σ_8). This shows how results can be dramatically different when performing a different analysis and the importance of having good quality data.

We conclude therefore that despite the data have room for β at the order of per mill, it is necessary to have better data to constrain this value better, since as shown in Fig. 5, we are only able to give upper limits for it at the 2- and $3-\sigma$ level.

ACKNOWLEDGEMENTS

The authors thank the anonimous referee whose comments helped to improve the scientific content of this work. FP is supported by an STFC postdoctoral fellowship.

References

Abramo L. R., Batista R. C., Liberato L., Rosenfeld R., 2007, J. Cosmology Astropart. Phys., 11, 12
Abramo L., Batista R., Liberato L., Rosenfeld R., 2009, Phys. Rev. D, 79, 023516
Anderson L., Aubourg E., Bailey S., Bizyaev D., Blanton M., et al., 2013, MNRAS, 427, 3435
Ascasibar Y., Yepes G., Gottlöber S., Müller V., 2004, MNRAS, 352, 1109
Bahcall N. A., Bode P., 2003, Astrophys. J., 588, L1
Bahcall N. A., Fan X.-h., 1998, Astrophys. J., 504, 1
Bahcall N. A., et al., 2003a, Astrophys. J. Suppl., 148, 243
Bahcall N. A., et al., 2003b, Astrophys. J., 585, 182
Bahcall N. A., Dong F., Hao L., Bode P., Annis J., Gunn J. E., Schneider D. P., 2003c, Astrophys. J., 599, 814
Barkana R., Loeb A., 2001, Phys. Rep., 349, 125
Bartelmann M., Huss A., Colberg J. M., Jenkins A., Pearce F. R., 1998, Astron. Astrophys., 330, 1
Bartelmann M., Doran M., Wetterich C., 2006, A&A, 454, 27
Basilakos S., 2003, ApJ, 590, 636

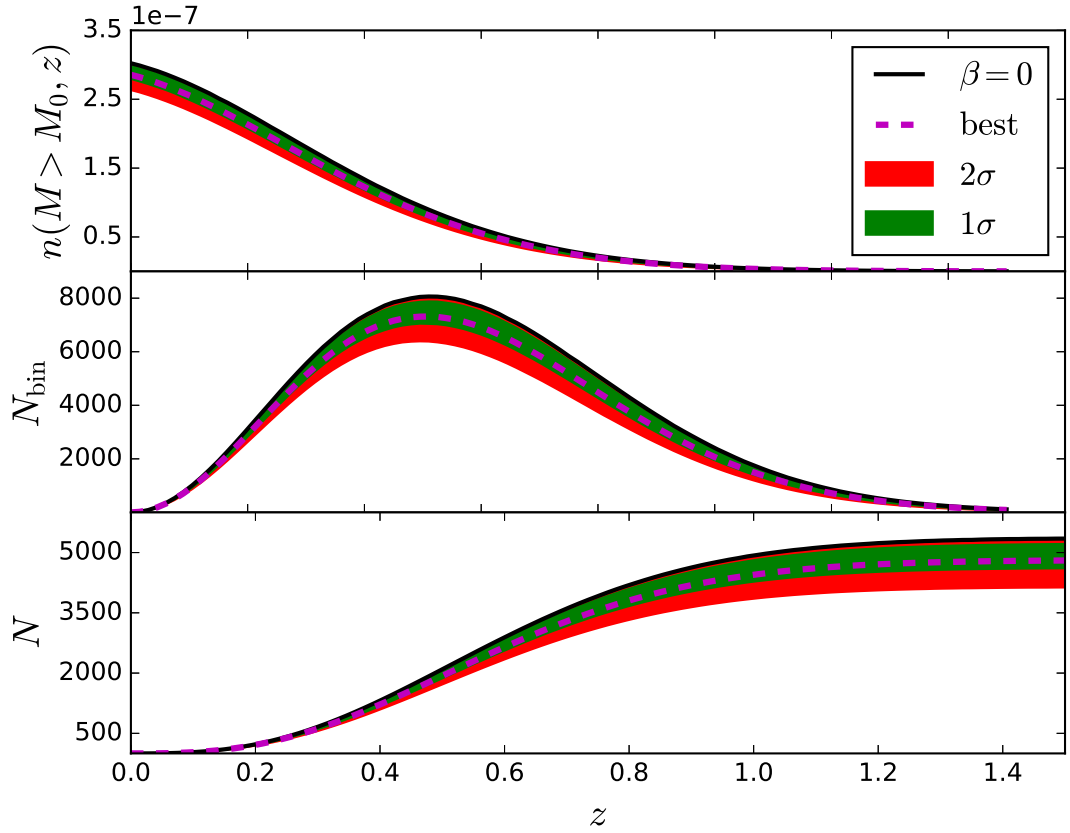

Figure 6. The computed comoving number density (top panel), the number of clusters in different redshift bins (middle panel) and total number of massive clusters (bottom panel) for the best fit value of β as well as the $1-\sigma$ and the $2-\sigma$ confidence regions. The magenta dashed line shows the best value and the black solid line is for the spherically symmetric case ($\beta = 0$).

Basilakos S., Voglis N., 2007, MNRAS, 374, 269
Basilakos S., Sanchez J. C. B., Perivolaropoulos L., 2009, Phys. Rev. D, 80, 043530
Basilakos S., Plionis M., Lima J. A. S., 2010, Phys. Rev. D, 82, 083517
Batista R. C., Pace F., 2013, JCAP, 6, 44
Bertschinger E., 1985, ApJS, 58, 39
Beutler F., Blake C., Colless M., Jones D. H., Staveley-Smith L., et al., 2011, MNRAS, 416, 3017
Blake C., Kazin E., Beutler F., Davis T., Parkinson D., et al., 2011, MNRAS, 418, 1707
Bond J. R., Cole S., Efstathiou G., Kaiser N., 1991, ApJ, 379, 440
Borgani S., et al., 2001, Astrophys. J., 561, 13
Bromm V., Yoshida N., 2011, ARA&A, 49, 373
Campanelli L., Fogli G. L., Kahniashvili T., Marrone A., Ratra B., 2012, European Physical Journal C, 72, 2218
Ciardi B., Ferrara A., 2005, Space Sci. Rev., 116, 625
Corless V. L., King L. J., 2009, Mon. Not. Roy. Astron. Soc., 396, 315
Corless V. L., King L. J., Clowe D., 2009, Mon. Not. Roy. Astron. Soc., 393, 1235
Dahle H., 2006, Astrophys. J., 653, 954
Del Popolo A., 2009, ApJ, 698, 2093
Del Popolo A., Gambera M., 1998, A&A, 337, 96
Del Popolo A., Gambera M., 1999, A&A, 344, 17
Del Popolo A., Pace F., Lima J. A. S., 2013a, International Journal of Modern Physics D, 22, 1350038
Del Popolo A., Pace F., Lima J. A. S., 2013b, Phys. Rev. D, 87, 043527
Del Popolo A., Pace F., Lima J. A. S., 2013c, MNRAS, 430, 628
Devi N. C., Choudhury T. R., Sen A. A., 2013, Mon. Not. Roy. Astron. Soc., 432, 1513
Donahue M., Voit G. M., Gioia I. M., Luppino G., Hughes J. P., Stocke J. T., 1998, Astrophys. J., 502, 550
Eisenstein D. J., Hu W., 1998, Astrophys. J., 496, 605
Engineer S., Kanekar N., Padmanabhan T., 2000, Mon. Not. Roy. Astron. Soc., 314, 279
Evrard A. E., et al., 2002, Astrophys. J., 573, 7
Fillmore J. A., Goldreich P., 1984, ApJ, 281, 1
Fosalba P., Gaztanaga E., 1998a, Mon. Not. Roy. Astron. Soc., 301, 503
Fosalba P., Gaztanaga E., 1998b, Mon. Not. Roy. Astron. Soc., 301, 535
Gaztanaga E., Fosalba P., 1998, Mon. Not. Roy. Astron. Soc., 301, 524
Gunn J. E., Gott J. R., 1972, ApJ, 176, 1
Guth A. H., 1981, Phys. Rev. D, 23, 347
Henry J. P., 2000, Astrophys. J., 534, 565
Hinshaw G., et al., 2013, ApJS, 208, 19
Hoffman Y., Shaham J., 1985, ApJ, 297, 16
Horellou C., Berge J., 2005, MNRAS, 360, 1393
Hu W., Sugiyama N., 1996, ApJ, 471, 542
Huang Q.-G., Wang K., Wang S., 2015, JCAP, 1512, 022
Ikebe Y., Reiprich T. H., Boehringer H., Tanaka Y., Kitayama T., 2002, Astron. Astrophys., 383, 773
Jenkins A., Frenk C. S., White S. D. M., Colberg J. M., Cole S., Evrard A. E., Couchman H. M. P., Yoshida N., 2001, Mon. Not. Roy. Astron. Soc., 321, 372
Klypin A. A., Trujillo-Gomez S., Primack J., 2011, ApJ, 740, 102
Li M., Li X. D., Wang S., Zhang X., 2009, J. Cosmology Astropart. Phys., 6, 036
Lima J., Zanchin V., Brandenberger R. H., 1997, MNRAS, 291, L1

Linde A., 1990, Physics Letters B, 238, 160
Lokas E. L., 2001, Acta Physica Polonica B, 32
Malekjani M., Naderi T., Pace F., 2015, Mon. Not. Roy. Astron. Soc., 453, 4148
Mantz A., Allen S. W., Rapetti D., Ebeling H., 2010, MNRAS, 406, 1759
Maor I., Lahav O., 2005, JCAP, 7, 3
Marciu M., 2016, Phys. Rev. D, 93, 063514
Meyer S., Pace F., Bartelmann M., 2012, Phys. Rev. D, 86, 103002
Mota D. F., van de Bruck C., 2004, A&A, 421, 71
Naderi T., Malekjani M., Pace F., 2015, MNRAS, 447, 1873
Navarro J. F., Frenk C. S., White S. D. M., 1997, ApJ, 490, 493
Nunes N. J., Mota D. F., 2006, MNRAS, 368, 751
Nusser A., 2001, Mon. Not. Roy. Astron. Soc., 325, 1397
Pace F., Waizmann J. C., Bartelmann M., 2010, MNRAS, 406, 1865
Pace F., Fedeli C., Moscardini L., Bartelmann M., 2012, MNRAS, 422, 1186
Pace F., Moscardini L., Crittenden R., Bartelmann M., Pettorino V., 2014a, MNRAS, 437, 547
Pace F., Batista R. C., Popolo A. D., 2014b, MNRAS, 445, 648
Padmanabhan N., Xu X., Eisenstein D. J., Scalzo R., Cuesta A. J., et al., 2012, MNRAS, 427, 2132
Peacock J. A., 1999, Cosmological Physics. Cambridge University Press
Peebles P. J. E., 1993, Principles of physical cosmology. Princeton University Press
Peebles P. J., Ratra B., 2003, Reviews of Modern Physics, 75, 559
Planck Collaboration XIII 2015, ArXiv e-prints, 1502.01589,
Prada F., Klypin A. A., Cuesta A. J., Betancort-Rijo J. E., Primack J., 2012, Mon. Not. Roy. Astron. Soc., 423, 3018
Press W. H., Schechter P., 1974, ApJ, 187, 425
Reed D., Gardner J., Quinn T. R., Stadel J., Fardal M., Lake G., Governato F., 2003, Mon. Not. Roy. Astron. Soc., 346, 565
Reed D., Bower R., Frenk C., Jenkins A., Theuns T., 2007, Mon. Not. Roy. Astron. Soc., 374, 2
Reiprich T. H., Boehringer H., 2002, Astrophys. J., 567, 716
Reischke R., Pace F., Meyer S., Schäfer B. M., 2016, MNRAS,
Ryden B. S., Gunn J. E., 1987, ApJ, 318, 15
Schuecker P., Böhringer H., Collins C. A., Guzzo L., 2003, A&A, 398, 867
Sheth R. K., Tormen G., 1999, MNRAS, 308, 119
Sheth R. K., Tormen G., 2002, MNRAS, 329, 61
Starobinsky A. A., 1980, Physics Letters B, 91, 99
Subramanian K., Cen R., Ostriker J. P., 2000, ApJ, 538, 528
Suzuki N., Rubin D., Lidman C., Aldering G., et.al 2012, ApJ, 746, 85
Vikhlinin A., et al., 2009a, ApJ, 692, 1033
Vikhlinin A., et al., 2009b, ApJ, 692, 1060
Wang P., 2006, Astrophys. J., 640, 18
Wang L., Steinhardt P. J., 1998, ApJ, 508, 483
White S. D. M., Rees M. J., 1978, MNRAS, 183, 341
Williams L. L. R., Babul A., Dalcanton J. J., 2004, ApJ, 604, 18
Wintergerst N., Pettorino V., 2010, Phys. Rev. D., 82, 103516
Zukin P., Bertschinger E., 2010a, Phys. Rev., D82, 104044
Zukin P., Bertschinger E., 2010b, Phys. Rev., D82, 104045